Inorganic Chemistry

Article

pubs.acs.org/IC

Syntheses, Structures, and Spectroscopic Properties of Plutonium and Americium Phosphites and the Redetermination of the Ionic Radii of Pu(III) and Am(III)

Justin N. Cross, Eric M. Villa, Shuao Wang, Juan Diwu, Matthew J. Polinski, and Thomas E. Albrecht-Schmitt*

Department of Chemistry and Biochemistry and Department of Civil Engineering and Geological Sciences, University of Notre Dame, 156 Fitzpatrick Hall, Notre Dame, Indiana 46556, United States

Supporting Information

ABSTRACT: A series of isotypic rare earth phosphites (RE = Ce(III), Pr(III), Nd(III), Pu(III), or Am(III)) with the general formulas $RE_2(HPO_3)_3(H_2O)$ along with a Pu(IV) phosphite, $Pu[(HPO_3)_2(H_2O)_2]$, have been prepared hydrothermally via reactions of $RECl_3$ with phosphorous acid. The structure of $RE_2(HPO_3)_3(H_2O)$ features a face-sharing interaction of eight- and nine-coordinate rare earth polyhedra. By use of the crystallographic data from the isotypic series along with data from previously reported isotypic series, the ionic radii for higher coordinate Pu(III) and Am(III) were calculated. The ^{VIII}Pu(III) radius was calculated as 1.112 ± 0.004 Å, and the ^{IX}Pu(III) radius was calculated to be 1.165 ± 0.002 Å. The ^{VIII}Am(III) radius was calculated as 1.108 ± 0.004 Å, and the ^{IX}Am(III) radius was calculated as 1.162 ± 0.002 Å.

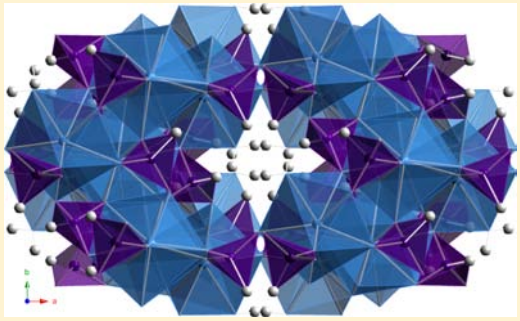

INTRODUCTION

Structural information on compounds containing transuranium elements is limited owing to the challenges in working with these radioactive elements. However, this data is essential in order to develop periodic trends and properties such as ionic radii, which are commonly used to guide inorganic synthesis and separation processes. Reliable ionic radii are of increased importance owing to the common use of surrogates such as Nd(III) for Pu(III) or Sm(III) for Am(III). The use of surrogates relies on matching the ionic radius of the actinide with a similarly sized lanthanide. Additionally, the design of advanced nuclear waste forms requires doping transuranics into different crystal lattices.[1−4] This requires matching the ionic radius of the cations so that substitution can take place while retaining the integrity of the solid matrix. Ionic radius varies dramatically with oxidation state and coordination number.[5] Due to the lack of structural information for the transuranic elements, the ionic radius values for Pu(III) and Am(III) with higher coordination vary widely.[6−11] The ionic radius is an average measure that can be used to approximate bond distances when charge and coordination of both cation and anion are taken into account. These values can be calculated by using the interatomic distances attained from oxide and fluoride crystal structures, plots of radii vs oxidation state, plots of radii vs coordination number, or plots of radii cubed vs unit cell volume as was performed in this paper.[5] In order to use this method, an isotypic series of compounds is needed where the majority of the structures contain ions that have well-defined values. The unknown values can be calculated from the linear r^3 vs V plot. In the past ten years, a few series of isotypic compounds with eight- and nine-coordinate cation centers have been synthesized, and crystallographic information is reported across the lanthanide and actinide series.[12−17] Typically, the crystal structure changes as the series is traversed, and the comparison can no longer be made as is the case with the series of nine-coordinate acetonitrile complexes.[18] The nine-coordinate rare earth triflate series $[RE(H_2O)_9][CF_3SO_3]_3$ has been synthesized and characterized for RE(III) = La, Ce, Pr, Nd, Sm, Eu, Gd, Tb, Dy, Ho, Er, Tm, Yb, Lu, U, Np, Pu, Am, Cm, and Cf.

Lanthanide phosphites have been reported previously with a number of different structure types, but to our knowledge this is the first systematic investigation of lanthanide phosphites from La to Eu.[19−24] Until recently there has been little work in the area of actinide phosphites despite the potential of phosphorous acid as an *in situ* reductant.[25−30] In the past year, our group has explored the redox chemistry of phosphite with actinides and reported a series of tetravalent actinide phosphites (Th(IV) to Np(IV)) and a family of compounds following the reduction of U(VI) to U(IV) and the oxidation of phosphite to phosphate.[31,32] Our study of the phosphite system continues with the synthesis of a series of trivalent isotypic rare earth phosphites with the formula $RE_2(HPO_3)_3(H_2O)$ (RE = Ce(III), Pr(III), Nd(III), Pu(III), and Am(III)), which are used to calculate ionic radii for eight- and nine-coordinate Pu(III)

Received: May 9, 2012
Published: July 17, 2012

   dx.doi.org/10.1021/ic300958z | *Inorg. Chem.* 2012, 51, 8419−8424

and Am(III) using r^3 vs unit cell volume plots. Additionally, we report the structure of a Pu(IV) phosphite that is isotypic with the Th(IV), U(IV), and Np(IV) phosphites with the formula $Pu[(HPO_3)_2(H_2O)_2]$ previously reported by us. Finally, we observe a transition in structure type across the lanthanide series between Nd(III) phosphite and Sm(III) phosphite with the formula $Ln[(HPO_3H)(HPO_3)(H_2O)]$.

EXPERIMENTAL SECTION

Syntheses. La_2O_3 (99.9%, Alfa Aesar), $CeCl_3$ (99.9%, Alfa Aesar), $PrCl_3{\cdot}xH_2O$ (99.9%, Alfa Aesar), $NdCl_3{\cdot}xH_2O$ (99.9%, Alfa Aesar), $SmCl_3{\cdot}xH_2O$ (99.9%, Alfa Aesar), $EuCl_3{\cdot}xH_2O$ (99.9%, Alfa Aesar), Na_2CO_3 (ACS reagent grade, Matheson Coleman Bell), and H_3PO_3 (97%, Alfa Aesar) were all used as obtained. Weapons-grade plutonium (94% ^{239}Pu, 6% ^{240}Pu) in the form of $PuCl_3$ was used as received from LANL. Americium (^{243}Am with trace ^{242}Am and ^{241}Am) in the form of AmO_2 was received from ORNL and used as obtained. Reactions were run in PTFE-lined Parr 4749 autoclaves with a 23 mL internal volume for the lanthanides and with 10 mL internal volume autoclaves for plutonium and americium. Deionized water was used in all reactions. ***Caution!*** *^{239}Pu ($t_{1/2}$ = 24,065 years), ^{240}Pu ($t_{1/2}$ = 6,537 years) and ^{243}Am ($t_{1/2}$ = 7370 years) represent serious health risks owing to their α and γ emission. All studies with plutonium and americium were conducted in a laboratory dedicated to studies on transuranium elements. This laboratory is located in a nuclear science facility and is equipped with HEPA filtered hoods and negative pressure gloveboxes that are ported directly into the hoods. A series of counters continually monitor radiation levels in the laboratory. The laboratory is licensed by the Nuclear Regulatory Commission. All experiments were carried out with approved safety operating procedures. All free-flowing solids are worked with in gloveboxes, and products are only examined when coated with either water or Krytox oil and water. There are significant limitations in accurately determining yield with plutonium and americium compounds because this requires drying, isolating, and weighing a solid, which poses certain risks, as well as manipulation difficulties given the small quantities employed in the reactions.*

$Pu(III)_2(HPO_3)_3(H_2O)$. $PuCl_3$ (0.0100 g, 0.029 mmol), Na_2CO_3 (0.0031 g, 0.029 mmol), and 200 μL of an argon-sparged 2 M H_3PO_3 solution (0.4 mmol) were loaded into a 10 mL autoclave. Na_2CO_3 was added because it was found that a slight increase in pH increased the yield. The autoclave was sealed and heated to 200 °C in a box furnace in an argon-filled glovebox for 2 h. The autoclave was then cooled to room temperature at a rate of 5 °C/h. The products were rinsed with water, and pale blue rhomboidal tablets were isolated.

$Pu(IV)[(HPO_3)_2(H_2O)_2]$. The purple mother liquor of the above reaction was isolated and exposed to oxygen. After 24 h pink fan-shaped crystals of $Pu[(HPO_3)_2(H_2O)_2]$ precipitated.

$Am_2(HPO_3)_3(H_2O)$. AmO_2 (0.0050 g, 0.018 mmol) was dissolved in 5 M HCl (150 μL) in an autoclave. The solution was dried by heating at 150 °C leaving a yellow solid of hydrated $AmCl_3$. Na_2CO_3 (0.0018 g, 0.017 mmol) and 150 μL of 2 M H_3PO_3 solution (0.3 mmol) were loaded into a 10 mL autoclave. The autoclave was sealed and heated to 200 °C in a box furnace for 2 h. The autoclave was then cooled to room temperature at a rate of 5 °C/h. The products were rinsed with water, and light pink hexagonal tablets of $Am_2(HPO_3)_3(H_2O)$ were isolated.

$Ln_2(HPO_3)_3(H_2O)$ and $Ln[(HPO_3H)(HPO_3)(H_2O)]$, Ln = La–Lu. All of the lanthanides were prepared from $LnCl_3$ or Ln_2O_3. The oxides were dissolved in a minimum amount of 5 M HCl (~400 μL) before being used. In a typical reaction, 0.2 mmol (metal basis) was loaded into a 23 mL autoclave with 4 mmol of 2 M H_3PO_3 solution. The autoclave was sealed and heated to 200 °C for 2 h then cooled to room temperature at a rate of 5 °C/h. The products were washed with water and isolated. Crystals in the form of rhomboidal tablets were collected for $Ln_2(HPO_3)_3(H_2O)$ (Ln = La, Ce, Pr, and Nd) and crystals in the form of columns or needles were collected for $Ln[(HPO_3H)(HPO_3)(H_2O)]$ (Ln = Sm, Eu, Gd, Tb, Dy, Ho, Er, Tm, Yb, and Lu).

Crystallographic Studies. Single crystals of $Pu_2(HPO_3)_3(H_2O)$, $Pu[(HPO_3)_2(H_2O)_2]$, $Am_2(HPO_3)_3(H_2O)$, $Ln_2(HPO_3)_3(H_2O)$ (Ln = La, Ce, Pr, and Nd), and $Ln[(HPO_3H)(HPO_3)(H_2O)]$ (Ln = Sm and Eu) phases were mounted in cryoloops with viscous Krytox and optically aligned on a Bruker APEXII CCD X-ray diffractometer or a Bruker APEXII Quazar X-ray diffractometer using a digital camera. Initial intensity measurements were either performed using an IμS X-ray source, a 30 W microfocused sealed tube (Mo Kα, λ = 0.71073 Å) with high-brilliance and high-performance focusing Quazar multilayer optics or a standard sealed tube with a monocapillary collimator. Standard APEXII software was used for determination of the unit cells and data collection control. The intensities of reflections of a sphere were collected by a combination of four sets of exposures (frames). Each set had a different φ angle for the crystal and each exposure covered a range of 0.5° in ω. A minimum of 1464 frames were collected with an exposure time per frame of 10–60 s, depending on the crystal. The SAINT software was used for data integration including Lorentz and polarization corrections. Semiempirical absorption corrections were applied using the program SADABS or TWINABS.[33]

UV–Vis–NIR Spectroscopy. UV–vis–NIR data were acquired from single crystals using a Craic Technologies microspectrophotometer. Crystals were placed on quartz slides under Krytox oil, and the data was collected from 400 to 1400 nm (see Supporting Information).

RESULTS AND DISCUSSION

Structures and Topological Descriptions. The isotypic series $RE_2(HPO_3)_3(H_2O)$ is a dense 3D framework based on face-sharing, edge-sharing, and corner-sharing RE^{3+} cation polyhedra along with edge- and corner-sharing polyhedra. The RE1 center is an eight-coordinate bicapped trigonal prism with approximate C_{2v} symmetry where seven coordinating oxygen atoms are shared with phosphite anions and the eighth oxygen atom is donated from a coordinating water molecule (O10).[38] The RE2 center is a nine-coordinated tricapped trigonal prism where all nine oxygen atoms are donated from phosphite anions. The two RE centers face-share through O2, O4, and O9 to form a dimer. The dimer then edge-shares with other dimers to form chains. The chains corner-share with each other to form the overall 3D framework containing cross-shaped channels running along the *c* axis as shown in Figure 1. This structure type was first reported by Xiong et al. for $La_2(HPO_3)_3(H_2O)$ only,[23] but the syntheses and crystal structures for Ln = Ce–Nd and An = Pu(III) and Am(III) are presented for the first time here. The lanthanide contraction is observed clearly in this series when the average Ln–O bond lengths are compared for both metal centers. There is an average difference of −0.020 Å between the lanthanides when the RE1–O distances are compared and an average difference of −0.018 Å when the RE2–O distances are compared. The crystallographic information for the actinide compounds are in Table 1, the crystallographic information for the lanthanide compounds are in Table 2, and selected bond distances for all $RE_2[(HPO_3)_3(H_2O)]$ compounds can be found in Table 3.

The Pu(IV) phosphite phase, $Pu[(HPO_3)_2(H_2O)_2]$, adopts a 3D structure based on corner-sharing between the Pu(IV) and P(III) polyhedra that can be seen in Figure 2. The PuO_8 moieties are trigonal dodecahedra with approximate D_{2d} symmetry where six oxygen atoms are donated from phosphite anions and two oxygen atoms are donated from coordinating water molecules.[38] The Pu(IV) phosphite is isotypic with the Th(IV), U(IV), and Np(IV) phosphite structures previously reported by our group.[31] This series exhibits the actinide contraction moving from Th(IV) phosphite to Pu(IV) phosphite. Looking at the average An–O distances (excluding $An–OH_2$), there is a −0.051 Å difference between Th(IV) and

dx.doi.org/10.1021/ic300958z | Inorg. Chem. 2012, 51, 8419–8424

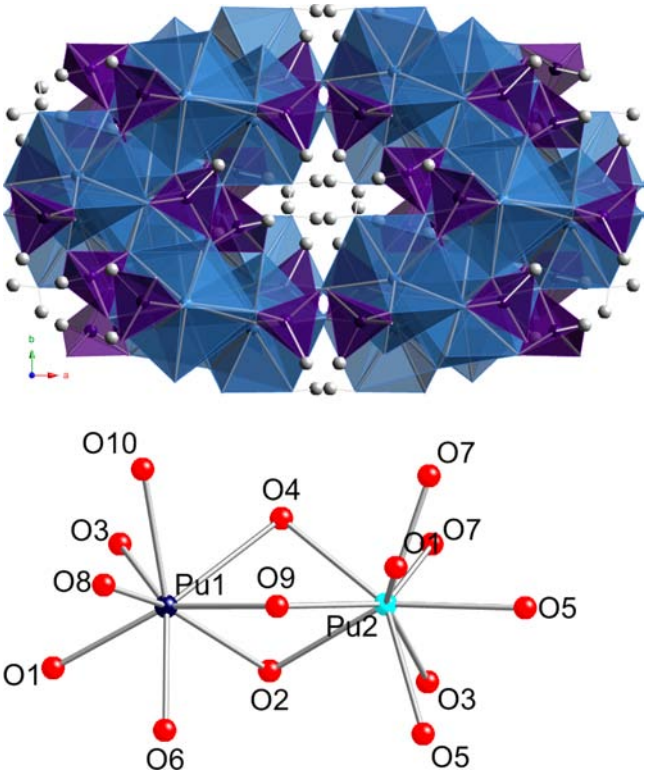

Figure 1. (top) View along the *c* axis of $RE_2[(HPO_3)_3(H_2O)]$ showing the star-shaped channels. RE polyhedra are blue, phosphite polyhedra are purple, and hydrogen atoms are white spheres. (bottom) The ball-and-stick model of the face-sharing dimer in the Pu(III) analogue. The Pu(III) centers are blue spheres and the oxygen atoms are red spheres.

U(IV), a −0.011 Å difference between U(IV) and Np(IV), and a −0.014 Å difference between Np(IV) and Pu(IV). It is of note that the actinide contraction is not always observed and depends on the coordination environment and the quality of the crystal data. The crystallographic information for this compound are in Table 1 and the bond distances are in Table 4.

In the lanthanide phosphite series, there is a change in structure type between neodymium and samarium. The later lanthanides (Sm−Lu) adopt the phase $Ln[(HPO_3H)(HPO_3)(H_2O)]$, which contains sheets of Ln distorted dodecahedra with approximate C_{2v} symmetry and phosphite anions separated by water molecules.[38] These compounds exhibit edge-sharing between cation polyhedra and between cation−anion polyhedra as shown in Figure 3. This structure type was previously reported by Clearfield for a cerium analogue but has not been reported for the later lanthanides.[19] Crystallographic data for these compounds are in Table 2 and selected bond distances are in Table 4. Further information on the crystal structures can be found in the Supporting Information.

UV−Vis−NIR Absorption Spectroscopy. The absorption spectra for $Pu(III)_2(HPO_3)_3(H_2O)$, $Pu(IV)[(HPO_3)_2(H_2O)_2]$, and $Am_2(HPO_3)_3(H_2O)$ were obtained from single or twinned crystals of each compound and are shown in Figure 4. The electronic transitions of f-elements are well-known and have been characterized in literature.[34−37] Because these transitions are f−f transitions, they change little with coordination environment and can be identified between vastly different compounds. Herein we employ Carnall's analysis of Pu(III), Pu(IV), and Am(III) of UV−vis−NIR absorption spectra to assign transitions. The absorbance spectra for Pu(III) and Pu(IV) phosphite can be seen in Figure 4 and display the signature peaks of their oxidation state. The $^4L_{13/2}$ and $^4M_{15/2}$ peaks around 600 nm along with the $^6H_{13/2}$ peaks around 900 nm are characteristic peaks for Pu(III). For Pu(IV), the $^5F_2$ + $^5I_6$ peaks centered at 1100 nm are indicative of the tetravalent state. At wavelengths less than 900 nm, the transitions are due to multiple J states and have not been deconvoluted, but the transitions match well with the spectra reported by Carnall.[37]

The absorption spectra of Am(III) as the crystalline halides have also been been thoroughly characterized by Carnall, and many of the electronic transitions can be assigned.[35] As seen in Figure 5, the major peak around 500 nm can be attributed to the $^5L_6$ and $^5D_2$ states. The peaks from 820 to 880 nm are from the $^7F_5$ and $^7F_6$ transitions. The lowest energy transition centered around 1050 nm is the $^7F_4$ transition.

Table 1. Crystallographic Data for $Pu_2[(HPO_3)_3(H_2O)]$, $Am_2[(HPO_3)_3(H_2O)]$, and $Pu[(HPO_3)_2(H_2O)_2]$

compound	$Pu_2[(HPO_3)_3(H_2O)]$	$Am_2[(HPO_3)_3(H_2O)]$	$Pu[(HPO_3)_2(H_2O)_2]$
formula mass	741.93	742.93	437.99
color and habit	pale blue, tablet	pale pink, tablet	bright pink, blades
space group	*C*2/*c*	*C*2/*c*	*Pbca*
a (Å)	20.6339(3)	20.5453(3)	8.651(2)
b (Å)	6.5947(1)	6.6076(1)	8.997(2)
c (Å)	13.8805(2)	13.8705(2)	18.227(5)
α (deg)	90	90	90
β (deg)	101.297(1)	101.4250(10)	90
γ (deg)	90	90	90
V (Å^3)	1852.18(5)	1845.68(5)	1418.7(7)
Z	8	8	8
T (K)	100	100	100
λ (Å)	0.71073	0.71073	0.71073
max 2θ (deg)	27.32	24.96	28.98
ρ_{calcd} (g cm^{-3})	5.307	5.34	4.101
μ(Mo Kα) (cm^{-1})	146.67	170.59	97.46
$R(F)$ for $F_o^2 > 2\sigma(F_o^2)^a$	0.0298	0.042	0.0177
$R_w(F_o^2)^b$	0.061	0.0688	0.0341

$^aR(F) = \sum||F_o| - |F_c||/\sum|F_o|$. $^bR_w(F_o^2) = [\sum[w(F_o^2 - F_c^2)^2]/\sum wF_o^4]^{1/2}$.

dx.doi.org/10.1021/ic300958z | *Inorg. Chem.* 2012, 51, 8419−8424

Table 2. Crystallographic Data for $Ln_2[(HPO_3)_3(H_2O)]$, and $Ln[(HPO_3H)(HPO_3)(H_2O)]$

compound	$Ce_2[(HPO_3)_3(H_2O)]$	$Pr_2(HPO_3)_3(H_2O)$	$Nd_2(HPO_3)_3(H_2O)$	$Sm(HPO_3H)\ (HPO_3)(H_2O)$	$Eu(HPO_3H)\ (HPO_3)(H_2O)$
formula mass	532.17	539.75	546.41	344.32	345.93
color and habit	colorless, tablet	pale green, tablet	pale purple, tablet	colorless, column	colorless, column
space group	$C2/c$	$C2/c$	$C2/c$	$P2_12_12_1$	$P2_12_12_1$
a (Å)	20.7260(3)	20.6579(3)	20.5551(3)	6.6369(2)	6.6138(2)
b (Å)	6.6709(1)	6.6379(1)	6.6084(1)	6.9771(2)	6.9620(2)
c (Å)	14.0222(2)	13.9532(2)	13.8781(2)	16.3921(4)	16.4075(4)
α (deg)	90	90	90	90	90
β (deg)	101.2480(10)	101.3530(10)	101.4680(10)	90	90
γ (deg)	90	90	90	90	90
V (Å^3)	1901.49(5)	1875.90(5)	1847.51(5)	759.06(4)	755.49(4)
Z	8	8	8	4	4
T (K)	100	100	100	100	100
λ (Å)	0.71073	0.71073	0.71073	0.71073	0.71073
max 2θ (deg)	27.51	30.49	27.54	31.64	30.51
ρ_{calcd} (g cm^{-3})	3.746	3.808	3.915	3.013	3.041
μ(Mo Kα) (cm^{-1})	99.95	108.14	116.73	81.59	87.27
$R(F)$ for $F_o^2 > 2\sigma(F_o^2)^a$	0.0242	0.0655	0.0406	0.0197	0.0337
$R_w(F_o^2)^b$	0.0635	0.1351	0.0588	0.0407	0.0656

$^aR(F) = \sum||F_o| - |F_c||/\sum|F_o|$. $^bR_w(F_o^2) = [\sum[w(F_o^2 - F_c^2)^2]/\sum wF_o^4]^{1/2}$.

Table 3. Selected Bond Distances for $RE_2[(HPO_3)_3(H_2O)]$

$RE_2[(HPO_3)_3(H_2O)]$	Ce^{3+}	Pr^{3+}	Nd^{3+}	Pu^{3+}	Am^{3+}
RE(1)−O(8)	2.405(4)	2.393(8)	2.377(7)	2.395(6)	2.400(13)
RE(1)−O(9)	2.422(4)	2.403(8)	2.401(6)	2.399(6)	2.397(13)
RE(1)−O(1)	2.432(4)	2.412(8)	2.408(6)	2.395(6)	2.400(12)
RE(1)−O(2)	2.495(4)	2.495(9)	2.460(6)	2.471(7)	2.468(12)
RE(1)−O(3)	2.507(4)	2.513(8)	2.483(6)	2.484(7)	2.479(12)
RE(1)−O(6)	2.517(5)	2.505(8)	2.490(7)	2.495(7)	2.465(15)
RE(1)−O(10)	2.550(6)	2.51(1)	2.522(8)	2.515(9)	2.516(15)
RE(1)−O(4)	2.820(4)	2.784(8)	2.761(6)	2.734(6)	2.744(12)
RE(2)−O(7)	2.460(4)	2.446(8)	2.431(6)	2.428(7)	2.421(13)
RE(2)−O(7)	2.489(4)	2.478(7)	2.451(7)	2.474(7)	2.457(13)
RE(2)−O(4)	2.497(4)	2.482(8)	2.471(7)	2.499(7)	2.467(12)
RE(2)−O(9)	2.534(4)	2.514(8)	2.493(6)	2.508(7)	2.494(12)
RE(2)−O(5)	2.537(4)	2.522(8)	2.492(6)	2.511(6)	2.516(13)
RE(2)−O(5)	2.555(4)	2.540(8)	2.509(7)	2.520(7)	2.525(13)
RE(2)−O(2)	2.606(4)	2.594(9)	2.582(6)	2.584(6)	2.585(12)
RE(2)−O(3)	2.638(4)	2.621(7)	2.610(7)	2.624(7)	2.615(13)
RE(2)−O(1)	2.668(4)	2.657(8)	2.637(7)	2.671(6)	2.630(12)
P(1)−O(6)	1.507(4)	1.504(8)	1.502(7)	1.514(7)	1.520(16)
P(1)−O(7)	1.531(4)	1.530(8)	1.530(7)	1.533(7)	1.551(13)
P(1)−O(3)	1.540(4)	1.519(8)	1.533(7)	1.543(7)	1.531(13)
P(2)−O(4)	1.524(4)	1.530(8)	1.520(7)	1.506(8)	1.522(12)
P(2)−O(2)	1.530(4)	1.530(8)	1.533(7)	1.532(7)	1.534(13)
P(2)−O(5)	1.547(4)	1.533(9)	1.557(6)	1.538(7)	1.538(13)
P(3)−O(8)	1.501(5)	1.509(9)	1.494(8)	1.504(7)	1.489(14)
P(3)−O(1)	1.534(4)	1.535(9)	1.530(6)	1.536(7)	1.536(13)
P(3)−O(9)	1.538(4)	1.536(8)	1.529(7)	1.546(7)	1.542(14)
RE(1)−RE(2)	3.9517(4)	3.9242(9)	3.8946(7)	3.8975(5)	3.891

Ionic Radii of Pu(III) and Am(III). The ionic radius of cations is largely affected by their coordination number and valence.[5] The ionic radii were calculated by using the slopes of unit cell volume (V) vs r^3 (r = ionic radius) plots of the isotypic phosphite phase $RE_2(HPO_3)(H_2)$ (RE = La, Ce, Pr, Nd) presented in this work and the isotypic triflate phase $[RE(H_2O)_9][CF_3SO_3]_3$ reported previously.[13−16] The curves for nine-coordinate V versus r^3 for $RE_2(HPO_3)_3(H_2O)$ are shown in Figure 6. The ionic radius for nine-coordinate Am(III) was found to be 1.162 ± 0.002 Å after averaging the calculated values from both series. The ^{IX}Pu(III) was calculated only using the phosphite series because the crystallographic data reported for $[Pu(H_2O)_9][CF_3SO_3]_3$ was smaller than that reported for $[Am(H_2O)_9][CF_3SO_3]_3$, which may be due to collection temperatures varying between the two.[13,14] The calculated ^{IX}Pu(III) ionic radius was 1.165 ± 0.002 Å, and the calculated ^{VIII}Pu(III) radius was 1.112 ± 0.004 Å. To test these values, r vs coordination number (CN) plots were constructed for both Pu(III) and Am(III). Both plots were linear with an R^2 value close to 1, indicating a good fit. A revised value for

dx.doi.org/10.1021/ic300958z | Inorg. Chem. 2012, 51, 8419−8424

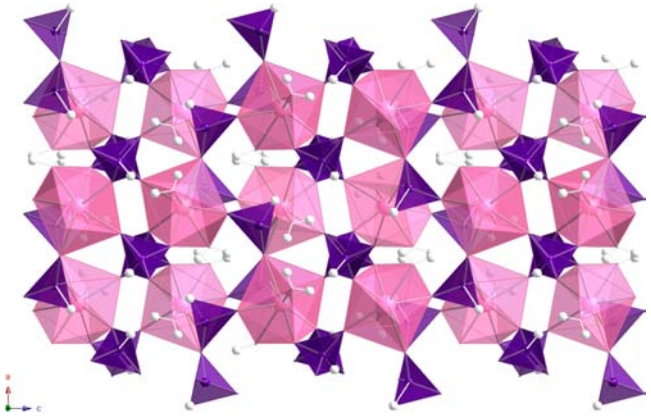

Figure 2. A view of the [*ac*] plane of $Pu[(HPO_3)_2(H_2O)_2]$ showing the 3D network formed by corner sharing between the Pu(IV) trigonal dodecahedra colored pink and the P(III) phosphite tetrahedra colored purple. Hydrogen atoms are displayed as white spheres.

Table 4. Selected Bond Distances for $Pu[(HPO_3)_2(H_2O)_2]$ and $Ln[(HPO_3H)(HPO_3)(H_2O)]$

$Pu[(HPO_3)_2(H_2O)_2]$	Pu^{4+}	$Ln[(HPO_3H)(HPO_3)(H_2O)]$	Sm^{3+}	Eu^{3+}
Pu(1)−O(7)	2.235(3)	Ln(1)−O(2)	2.311(2)	2.284(4)
Pu(1)−O(3)	2.246(3)	Ln(1)−O(1)	2.406(3)	2.388(5)
Pu(1)−O(4)	2.273(3)	Ln(1)−O(4)	2.415(2)	2.400(5)
Pu(1)−O(1)	2.290(3)	Ln(1)−O(3)	2.415(2)	2.408(5)
Pu(1)−O(2)	2.335(3)	Ln(1)−O(6)	2.422(3)	2.418(6)
Pu(1)−O(5)	2.344(3)	Ln(1)−O(5)	2.440(2)	2.422(5)
Pu(1)−O(8)	2.449(3)	Ln(1)−O(6)	2.498(2)	2.490(5)
Pu(1)−O(6)	2.490(3)	Ln(1)−O(1)	2.517(2)	2.503(5)
P(2)−O(2)	1.510(3)	P(1)−O(2)	1.517(2)	1.522(5)
P(2)−O(3)	1.521(3)	P(1)−O(6)	1.536(3)	1.531(5)
P(2)−O(1)	1.523(3)	P(1)−O(1)	1.537(3)	1.537(5)
P(3)−O(7)	1.518(3)	P(2)−O(3)	1.514(2)	1.518(6)
P(3)−O(5)	1.519(3)	P(2)−O(5)	1.516(3)	1.525(5)
P(3)−O(4)	1.521(3)	P(2)−O(7)	1.569(2)	1.575(6)

^{VIII}Am(III) was calculated as 1.108 ± 0.004 Å and using this value in the *r* vs CN plot of Am(III) gave a higher R^2 value showing it to be a valid method of determining ionic radii. Additionally, the lanthanide ionic radii were calculated in the same way, and the values calculated matched the values previously reported.[6] The first published ^{IX}Am(III) radius was 1.038 Å reported by Zachariasen followed by a radius of 1.034 Å reported by Milligan.[10,11] More recently, David has published radii for ^{VIII}Am(III), ^{IX}Am(III), ^{VIII}Pu(III), and ^{IX}Pu(III) of 1.106, 1.169, 1.123, and 1.187 Å, respectively from studies of the aquo complexes.[8,9] These values are closer to the values calculated here. The ^{VIII}Am(III) radii reported by David and in this paper are slightly larger than the value reported by Shannon, 1.09 Å. Similarly, the ^{IX}Am(III) radii reported by David and in this paper are significantly larger than the older values and seem more reasonable. Both Am(III) and Pu(III) ionic radii are quite close to the Nd(III) ionic radius showing that Nd(III) is the best surrogate for either Am(III) or Pu(III).

CONCLUSIONS

An isotypic series of rare earth phosphites with the formula $RE_2(HPO_3)_3(H_2O)$ (RE = Ce(III), Pr(III), Nd(III), Pu(III), or Am(III)) has been synthesized. Using the crystallographic information from this series along with previously reported structures, we calculated new ionic radii for higher coordinate Pu(III) and Am(III). The ^{VIII}Am(III) radius was calculated as 1.108 ± 0.004 Å, and the ^{IX}Am(III) radius was calculated as 1.162 ± 0.002 Å. The ^{VIII}Pu(III) radius was calculated as 1.112 ± 0.004 Å, and the ^{IX}Pu(III) radius was calculated as 1.165 ± 0.002 Å. These new values should help guide future design of advanced nuclear waste materials and separation processes. A

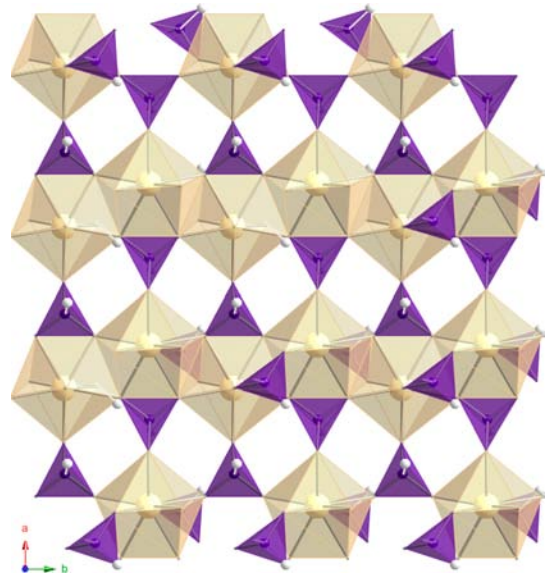

Figure 3. View along the [*ab*] plane of $Ln[(HPO_3H)(HPO_3)(H_2O)]$. Edge sharing between the cation dodecahedra colored gold and the phosphite tetrahedra colored purple is shown. Water molecules separate the sheets.

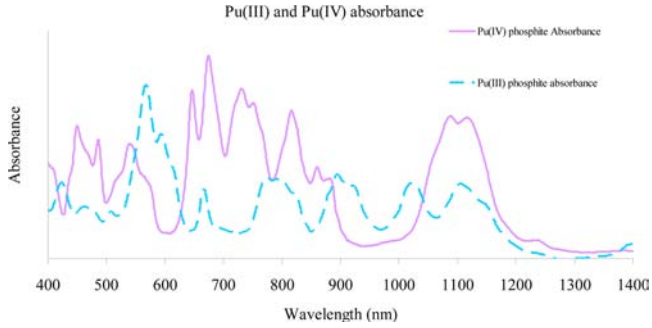

Figure 4. Absorbance spectra of Pu(III) phosphite (solid purple) and Pu(IV) phosphite (dotted blue). The Pu(III) peak centered around 900 nm is indicative of the trivalent state in Pu.

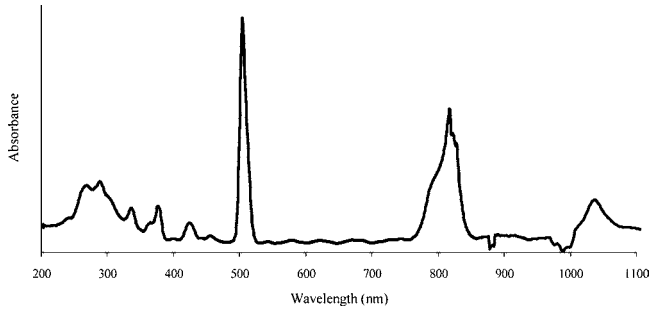

Figure 5. Absorbance spectra of Am(III) phosphite. The major peak centered around 500 is from the $^5L_6$ and $^5D_2$ transitions. The major peak around 800 nm is from the $^7F_5$ and $^7F_6$ transitions.

dx.doi.org/10.1021/ic300958z | *Inorg. Chem.* 2012, 51, 8419−8424

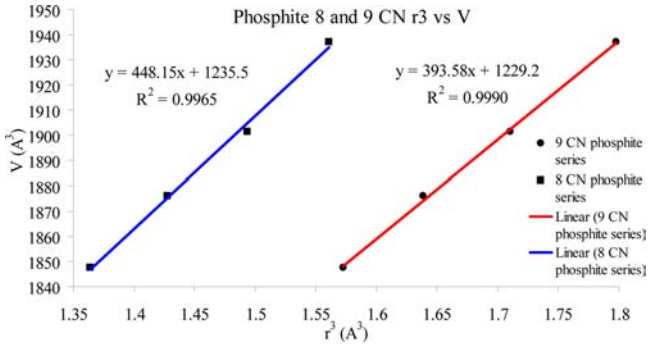

Figure 6. Plots of r^3 vs V for the isotypic phosphite series for eight- and nine-coordinate cations used to calculate the ionic radii of Pu(III) and Am(III). Using the fitted equation, where y is V and x is r^3, and the experimental unit cell volume of $[Am(H_2O)_9][CF_3SO_3]_3$ and $Am_2[(HPO_3)_3(H_2O)]$, we calculated the ^{IX}Am(III) radius as 1.162 ± 0.002 Å and the ^{VIII}Am(III) radius as 1.108 ± 0.004 Å. The ^{VIII}Pu(III) radius was calculated as 1.112 ± 0.004 Å, and the ^{IX}Pu(III) radius was calculated as 1.165 ± 0.002 Å.

change in structure type with the formula $Ln[(HPO_3H)(HPO_3)(H_2O)]$ is observed in the lanthanide series between Nd and Sm. In addition to the Pu(III) phosphite, a Pu(IV) phosphite was synthesized and found to be isotypic with our previously reported Th(IV), U(IV), and Np(IV) phosphites.

■ ASSOCIATED CONTENT

Ⓢ Supporting Information

Additional crystallographic images and information, photographs of the crystals, and additional plots. This material is available free of charge via the Internet at http://pubs.acs.org.

■ AUTHOR INFORMATION

Corresponding Author

*E-mail: talbrec1@nd.edu. Fax: (+01)574-631-9236.

Notes

The authors declare no competing financial interest.

■ ACKNOWLEDGMENTS

We are grateful for support provided by the Materials Science of Actinides, an Energy Frontier Research Center funded by the U.S. Department of Energy, Office of Science, Office of Basic Energy Sciences under Award Number DE-SC0001089.

■ REFERENCES

(1) Krivovichev, S. *Minerals as Advanced Materials I*; Springer: Heidelberg, Germany, 2008.
(2) Farnan, I.; Cho, H.; Weber, W. J. *Nature* **2007**, *445*, 190.
(3) Ewing, R. C. *Nature* **2007**, *445*, 161.
(4) Ewing, R. C. *Proc. Natl. Acad. Sci. U.S.A.* **1999**, *96*, 3432.
(5) Shannon, R. D.; Prewitt, C. T. *Acta Crystallogr.* **1969**, *B25*, 925.
(6) Shannon, R. D. *Acta Crystallogr.* **1976**, *A32*, 751.
(7) Rizkalla, E. N.; Choppin, G. R. Lanthanides and Actinides Hydration and Hydrolysis. In *Handbook on the Physics and Chemistry of Rare Earths. Lanthanides/Actinides: Chemistry*; Gschneidner, K. A., Jr., Eyring, L., Choppin, G. R., Lander, G. H., Eds.; Elsevier Science: Amsterdam, 1994; Vol. *18*, pp 529–558.
(8) David., F. H. *J. Less Common Met.* **1986**, *121*, 29.
(9) David, F. H.; Fourest, B. *New J. Chem.* **1997**, *21*, 167–176.
(10) Milligan, W. O.; Mullica, D. F.; Oliver, J. D. *J. Appl. Crystallogr.* **1979**, *12*, 411–412.
(11) Zachariasen, W. H. *Phys. Rev.* **1948**, *73*, 1104–1105.
(12) McB., J.; Harrowfield, D. L.; Kepert, J. M.; Patrick, A. H.; White. *Aust. J. Chem.* **1983**, *36*, 483–492.
(13) Lindqvist-Reis, P.; Apostolodis, C.; Rebizant, J.; Morgenstern, A.; Klenze, R.; Walter, O.; Fanghänel, T.; Haire, R. G. *Angew. Chem., Int. Ed.* **2007**, *46*, 919–922.
(14) Apostolodis, C.; Schimmelpfennig, B.; Magnani, N.; Lindqvist-Reis, P.; Walter, O.; Sykora, R. E.; Morgenstern, A.; Colineau, E.; Caciuffo, R.; Klenze, R.; Haire, R. G.; Rebizant, J.; Bruchertseifer, F.; Fanghänel, T. *Angew. Chem., Int. Ed.* **2010**, *49*, 6343–6347.
(15) Skanthakumar, S.; Antonio, M. R.; Wilson, R. E.; Solderholm., L. *Inorg. Chem.* **2007**, *46*, 3485–3491.
(16) Douglas, P.; Hector, A. L.; Levanson, W.; Light, M. E.; Matthews, M. L.; Webster, M. *Z. Anorg. Allg. Chem.* **2004**, *630*, 479–483.
(17) Sykora, R. E.; Assefa, Z.; Haire, R. G.; Albrecht-Schmitt, T. E. *Inorg. Chem.* **2005**, *44*, 5667–5676.
(18) Enriquez, A. E.; Matonic, J. H.; Scott, B. L.; Neu., M. P. *Chem. Commun.* **2003**, 1892–1893.
(19) Zhang, Y.; Hu, H.; Clearfield., A. *Inorg. Chim. Acta* **1992**, *193*, 35–42.
(20) Foulon, P. J.-D.; Tijani, N.; Durand, J.; Rafiq, M.; Cot., L. *Acta Crystallogr.* **1993**, *49*, 1–4.
(21) Foulon, P. J.-D.; Cot., L. *Acta Crystallogr.* **1995**, *C51*, 348–350.
(22) Ewald, B.; Prots, Y.; Kniep, R. *Z. Kristallogr.* **2005**, *220*, 533–534.
(23) Xiong, D.-B.; Li, M.-R.; Liu, W.; Chen, H.-H.; Yang, X.; Zhao., J.-T. *J. Solid. State. Chem.* **2006**, *179*, 2571–2577.
(24) Xiong, D.-B.; Zhang, Z.-J.; Gulay, L. D.; Tang, M.-B.; Chen, H.-H.; Yang, X.; Zhao., J.-T. *J. Inorg. Chim. Acta.* **2009**, *362*, 3013–3018.
(25) Chretien, A.; Kraft, J. C. *R. Hebd. Seances Acad. Sci.* **1937**, *204*, 1936.
(26) Avduevskaya, K. A.; Rozanov, I. A.; Mironova, V. S. *Inorg. Mater.* **1977**, *13*, 1515.
(27) Avduevskaya, K. A.; Ragulina, N. B.; Rozanov, I. A. *Inorg. Mater.* **1981**, *17*, 834.
(28) Doran, M.; Walker, S. M.; O'Hare, D. *Chem. Commun.* **2001**, 1988.
(29) Xu, J. F.; Li, H. H.; Cao, Y. N.; Huang, C. C.; Zhang, H. H.; Lin, D. S.; Yang, Q. Y.; Sun, R. Q. *Chin. J. Struct. Chem.* **2006**, *25*, 1380.
(30) Mandal, S.; Chandra, M.; Natarajan, S. *Inorg. Chem.* **2007**, *46*, 7935.
(31) Villa, E. M.; Wang, S.; Alekseev, E. V.; Depmeier, W.; Albrecht-Schmitt, T. E. *Eur. J. Inorg. Chem.* **2011**, *25*, 3749–3754.
(32) Villa, E. M.; Marr, C. J.; Jouffret, L. J.; Alekseev, E. V.; Depmeier, W.; Albrecht-Schmitt, T. E. *Inorg. Chem.* **2012**, *51*, 6548–6558.
(33) Sheldrick, G. M. SADABS, Program for absorption correction using SMART CCD based on Blessing's method. Blessing, R. H. *Acta Crystallogr.* **1995**, *A51*, 33.
(34) Pappalardo, R. G.; Carnall, W. T.; Fields, P. R. *J. Chem. Phys.* **1969**, *51*, 842.
(35) Pappalardo, R. G.; Carnall, W. T.; Fields, P. R. *J. Chem. Phys.* **1969**, *51*, 1182.
(36) Pappalardo, R. G.; Carnall, W. T.; Fields, P. R. *J. Chem. Phys.* **1970**, *53*, 2922.
(37) Carnall, W. T.; Liu, G. K.; Williams, C. W.; Reid, M. F. *J. Chem. Phys.* **1991**, *95*, 7194.
(38) Gorden, A. E. V.; Xu, J.; Raymond, K. N. *Chem. Rev.* **2003**, *103*, 4207.